J Appl Electrochem (2014) 44:807–820
DOI 10.1007/s10800-014-0686-y

RESEARCH ARTICLE

Nickel electrodeposition using EnFACE

Tri Widayatno · Sudipta Roy

Received: 13 December 2013 / Accepted: 17 March 2014 / Published online: 28 March 2014

Abstract In this paper, the usefulness of EnFACE "maskless" technology to transfer millimetre and micro scale features of nickel has been described. Here, electrode position was used with a patterned tool (anode) and uncoated substrate (cathode) placed in an electrochemical reactor separated by a narrow gap i.e. 300 μm. It requires resistive electrolytes with low concentration of metal ions which leads to a reduction of material and chemical usage. An electrochemical cell with a volume about 500 ml was utilised. An electrolyte of 0.19 M nickel sulfamate was chosen and shown to be capable of depositing nickel. Millimetre and micron scale feature manually fabricated as well as micron feature prepared by using photolithography were used. Current density for nickel deposition was observed to be different for each feature area. Nickel was deposited at cell potential ranging between −2.2 and −2.4 V. A feature of 1 mm × 5 mm and features of 300–800 μm width have been successfully transferred. An increase in dimension of the deposited feature was observed due to current spreading. The features were broader at longer processing time and for smaller feature size. A thickness up to 0.54 μm was obtained for 125–600 s at a current efficiency ranged between 50 and 90 %. EDX and XPS analysis show that the nickel deposit was metallic. SEM analysis shows that the deposited nickel was dense and compact.

T. Widayatno (✉) · S. Roy
School of Chemical Engineering and Advanced Materials, Newcastle University, Merz Court, Newcastle upon Tyne NE1 7RU, UK
e-mail: tri.widayatno@ums.ac.id

Keywords Electrodeposition · Enface technology · Pattern transfer · Nickel plating · Maskless patterning process

1 Introduction

Microfabricated devices with dimensions ranging between 0.05 to 500 μm are used in a wide range of industries [1–4]. Currently, the standard platform technology to manufacture such devices is photolithography [1, 2]. Photolithography requires substrates to be coated with a photosensitive resist. The resin-coated substrate is then exposed to ultraviolet (UV) light through a patterned mask. After development, metallic pattern transfer is attained by either plating or etching [1, 2]. The standard photolithographic method is a multi-step process, requires a clean room, and generates carbonaceous waste [1, 2, 5]. One possible method to minimise these problems is by achieving pattern transfer without using photolithography of each individual substrate [6].

Such a "maskless" pattern transfer process, Enface (Electrochemical nano and micro-fabrication by Flow and Chemistry), has been proposed recently [5–11]. Here, a desired pattern is defined on an electrochemical tool (*c.f.* Fig. 1). The tool and substrate are two electrodes in an electrochemical reactor separated by a narrow gap (300 μm) [7, 8]. Patterns on the tool can be transferred on to the substrate by imposing a current or voltage [7, 8], provided that the electrolyte resistance is high [5, 7, 8]. Since multiple substrates can be patterned using a single tool, use of photolithography can be greatly reduced [5, 7, 8]. In addition, it requires resistive electrolytes with low concentration of metal ions which reduces material and chemical usage [5, 7–11].

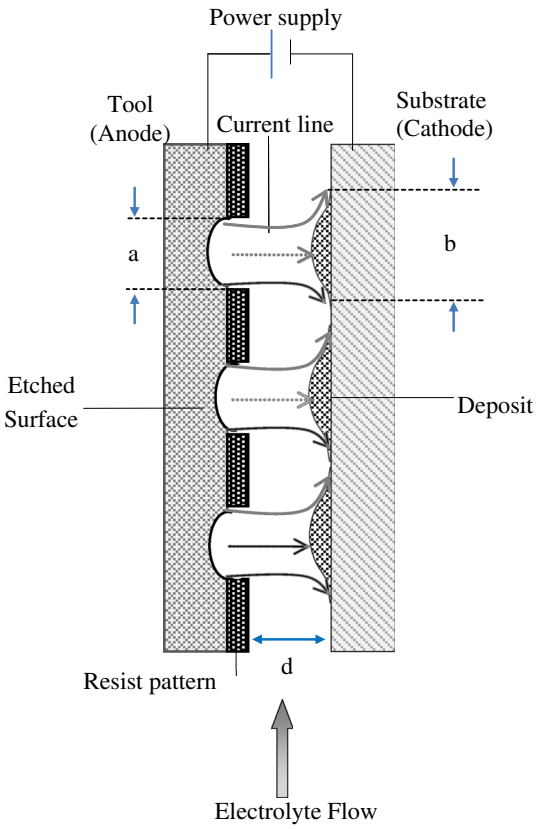

Fig. 1 Schematic illustration of Enface patterning process, *arrows* from anode to cathode illustrate the current line spread, *a* is the original feature width, *b* indicates the deposited feature width, and *d* is the distance between the electrodes

In this work, the usefulness of Enface technology for nickel deposition has been investigated. Nickel plating has been chosen due to its use in microelectronics [12–15], electroforming [16, 17] and other coatings [16, 18]. For these applications, nickel is deposited from sulfamate [16, 19–21], sulfamate-chloride [16, 19, 22], or sulphate [16, 22] electrolytes containing high concentration of Ni(II) ions, i.e., 0.7–1.4 mol dm^{-3} [16, 22]. In addition, nickel plating is not controlled by mass transfer, but by a combination of kinetics and mass transfer, in conditions where Enface has never been applied before. Earlier studies of Enface have focused on the etching and the deposition of copper, which is mass transfer controlled, from relatively dilute copper solutions under forced convection [7–9]. This is the first study on pattern transfer where metal deposition is controlled by kinetics and mass transfer.

Properties of deposited nickel have been shown to be dependent on electrolyte composition [23, 24], therefore a formulation of electrolyte is a crucial step. A step by step approach for formulating electrolytes that are applicable for pattern transfer of nickel using Enface method has been performed. The selected electrolyte is used to transfer patterns in an electrochemical cell with no external agitation. Millimetre and micrometre scale pattern features have been used to determine if pattern transfer can be achieved under these conditions.

2 Fundamental considerations

Earlier experiments and analysis have shown that pattern transfer for copper was achievable using an electrolyte conductivity of ≈ 0.27 S dm^{-1} [5, 8]. As nickel sulfamate and nickel chloride are nearly fully ionised in solution [25–27], the concentration of the salts to be dissolved in solution to maintain conductivity at this low range was estimated from the standard conductance equation for a fully ionised solution [28]

$$\kappa = c_+ \upsilon_+ \lambda_+ + c_- \upsilon_- \lambda_- \quad (1)$$

In Eq. 1, κ is electrolyte conductivity (S dm^{-1}), c is concentration of ions (mol dm^{-3}), λ is ionic conductivity (S dm^2 mol^{-1}), and the number of moles of cations υ_+ and anions υ_- released from one mole dissolved electrolyte. Using ionic conductivities of cation and anion involved in the electrolytes obtained from literature [28], as shown in Table 1, the concentration of nickel in solution needs to be within 0.15–0.2 mol dm^{-3} for sulfamate to remain within the range where solution resistivity will enable pattern transfer to occur.

Existing thermodynamic (i.e. Pourbaix) diagrams (Fig. 2) show that in order to obtain metallic nickel, a pH lower than 7.5 [22, 29] is required. However at very low pH (pH < 4), hydrogen evolution is facile which can lead to low current efficiency [30], and rise of pH near the electrode surface [22] leading to non-metallic deposit or oxide [22, 30]. In order to deposit metallic nickel a solution pH between 4 and 7.5 is required.

Nickel deposition is known to occur through several steps [19, 31–33]. A mechanism proposed for un-buffered electrolytes is [31, 34–37]:

$$Ni^{2+} + H_2O \rightleftarrows Ni(OH)^+ + H^+ \quad (2)$$

$$Ni(OH)^+ + e^- \rightleftarrows Ni(OH)_{ads} \quad (slow) \quad (3)$$

$$Ni(OH)_{ads} + Ni^{2+} + 2e^- \rightarrow Ni + Ni(OH)_{ads} \quad (4)$$

$$Ni(OH)_{ads} + e^- \rightarrow Ni + OH^- \quad (5)$$

Reaction (2) describes a homogeneous chemical reaction leading to the formation of an intermediate ($Ni(OH)^+$). A slow electron transfer (3) simultaneously takes place with an adsorption of its product preceding two parallel fast electron transfer reactions (4 and 5) to form metallic nickel [19, 31–33, 38–40]. Adsorbed protons may also discharge in parallel [16, 22, 30, 31, 33].

Table 1 Ionic conductivity (λ/S dm^2 mol^{-1}) of ions involved in the electrolytes, calculated and measured conductivities, and pH for the selected nickel solution with a measurement error of 1.3–2.2 %

Ion	λ_+/λ_-	Electrolyte	Calculated conductivity (S dm^{-1})	Experimental data (20 ± 2 °C)	
				Conductivity (S dm^{-1})	pH
H_3O^+	3.50	0.19 M $Ni(SO_3{\cdot}NH_2)_2$	0.28	0.22 ± 0.01	6.70 ± 0.22
Ni^{2+}	0.5				
$(SO_3{\cdot}NH_2)^-$	0.48				

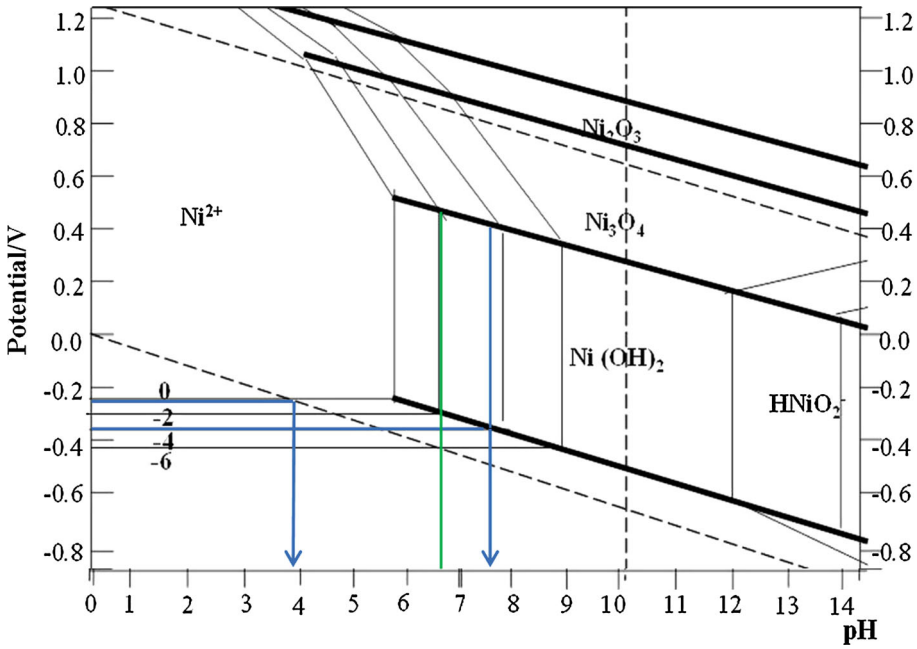

Fig. 2 *E*–pH diagram for nickel–water system (298 K)

$$H^+ + e^- \rightarrow H_{ads} \quad (6)$$

$$2H_{ads} \rightarrow H_2 \quad (7)$$

$$Ni(OH)_{ads} + H_{ads} + e^- \rightarrow Ni + H_{incl} + OH^- \quad (8)$$

Reactions (6), (7), and 8 evolve hydrogen or cause hydrogen to be included in Ni. Not only can hydrogen be included into the nickel deposit causing embrittlement [19, 30], but also increase in pH can lead to deposition of nickel oxide or hydroxide [33, 41]. Since the pH of nickel sulfamate electrolytes has been reported to be in the range of 6–7 [42], an electrolyte solutions containing 0.19 mol dm^{-3} nickel sulfamate was chosen. For such an electrolyte, the hydrogen evolution would be low and metallic nickel would be deposited.

3 Experimental

3.1 Electrolyte formulation

Electrolytic solutions of 0.19 mol dm^{-3} nickel sulfamate were prepared from analytical grade of nickel sulfamate in high purity deionised water i.e. 18 MΩ. To obtain the solution, a 62.6 g of $Ni(SO_3NH_2)_2.4H_2O$ (≥98 %, Sigma-Aldrich) was added into a 1.0 dm^3 deionised water while the solution was continuously stirred so that the chemical was fully dissolved. An S47 SevenMulti^{TM} dual pH and conductivity meter from Mettler-Toledo was employed in measuring pH and conductivity at ambient temperatures (20 ± 2 °C). The measurement of pH and conductivity was carried out for each new solution to ensure similar physicochemical properties were obtained. The pH and conductivity were also measured prior to and after each set of experiments to check whether there was a significant change during the deposition process.

3.2 Electrochemical cell

A cylindrical electrochemical cell was used for polarisation and pattern transfer experiments. The cell was constructed of polyvinyl chloride (PVC). The body of the cell was a PVC cylinder of 10 cm diameter and a depth of 8 cm (Fig. 3a). The cell had two polytetrafluoroethylene (PTFE) electrode holders on each side for locating the tool and the substrate (Fig. 3b). An inter-electrode gap of approximately 300 μm between the two electrodes

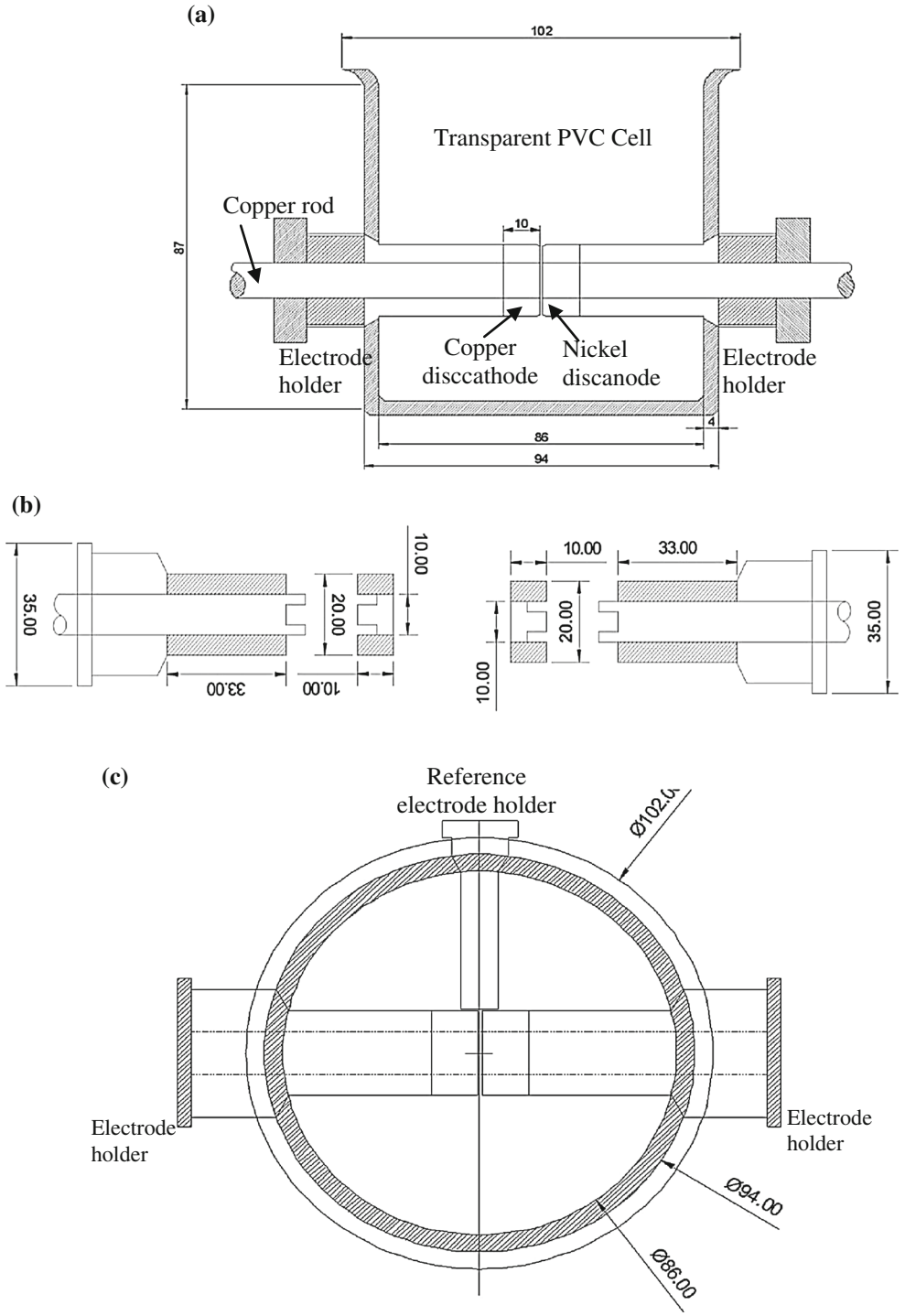

Fig. 3 Schematic diagram of cylindrical cell for Enface process with a volume of approximately 600 ml and dimensions in millimetre **a** side view, **b** electrode holders, **c** top view

was used for patterning experiments as recommended by previous works [7, 8]. This was achieved by pushing the electrodes forward by a screw action. A copper rod in the core of the electrode holder connected the electrodes to a power supply, and the electrode discs are mounted to the electrode holder by bolting them on with a head screw so only their front surface faced to the solution. About 500 ml of electrolyte was used to fill up the cell, which ensured that the electrodes were fully immersed.

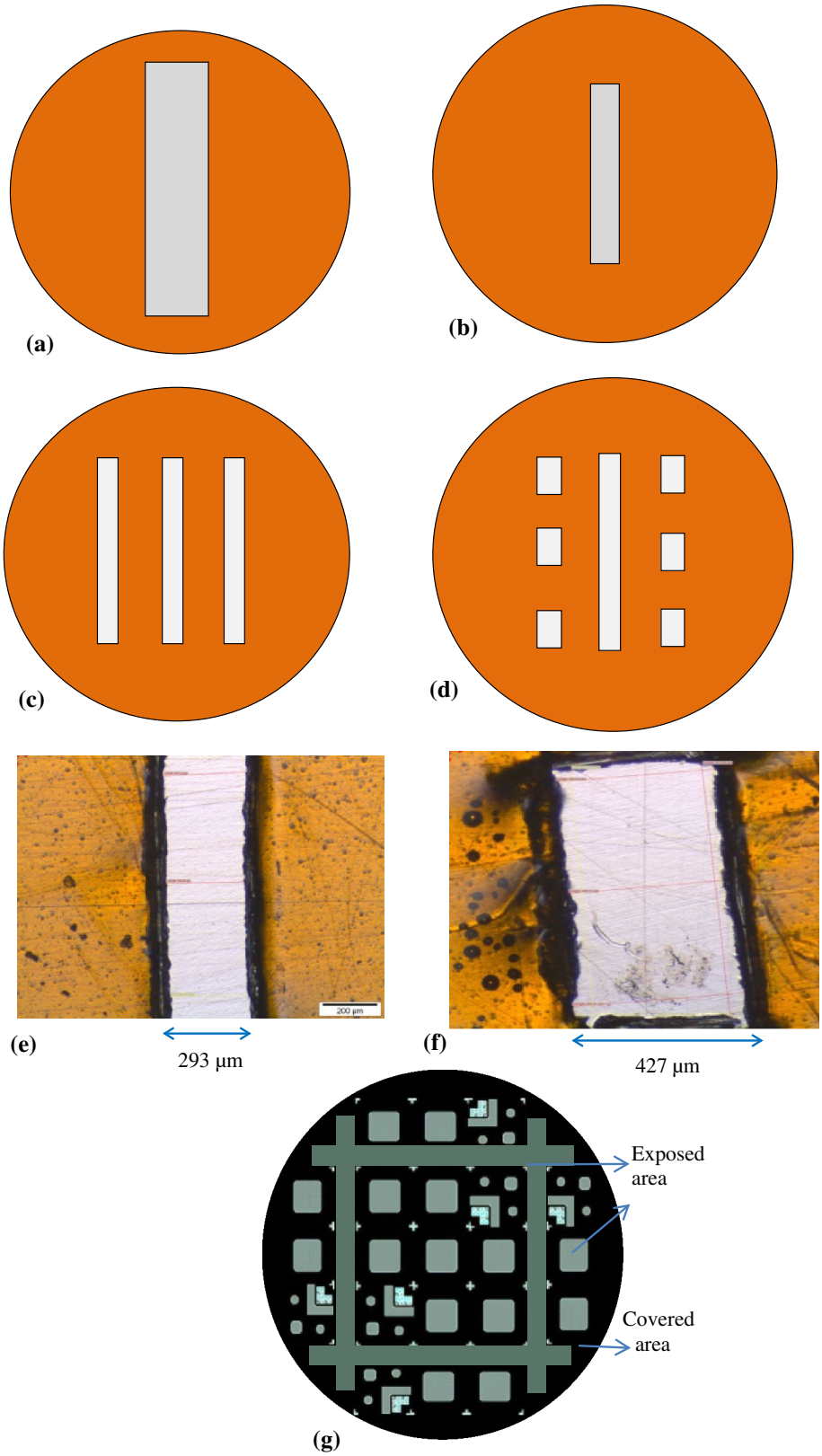

Fig. 4 Patterned anodes—manually fabricated feature of **a** 4 mm × 8 mm, **b** 1 mm × 5 mm **c** micron scale structure 1 **d** micron scale structure 2, **e** and **f** optical micrograph of features on the anode prepared by using Kapton tape—linear and rectangular features respectively, **g** micron scale pattern features fabricated by photolithography

The cathodes were polished copper discs of 1.0 cm diameter. The anodes, which served as the electrochemical tool, were fabricated from 1 cm diameter polished nickel discs. Both copper and nickel discs were of purity of 99.99 % (Goodfellow). A platinum wire (Goodfellow) reference was fabricated by inserting it in PTFE holder.

This was located orthogonally to the two electrodes (Fig. 3c). This reference electrode was placed at a close proximity of approximately 3–5 mm away from the cathode.

3.3 Electrode preparation

Each electrode was polished to a mirror finish using silicon carbide papers with grit sizes of #2400 and #4000 (Struers Dap-7). After polishing, the electrodes were washed by using deionised water and acetone to remove impurities. In a first set of experiments, each anode was prepared by covering the entire surface using a resistive material (Kapton tape, RS Components) of a thickness of 65 μm. A single feature of millimetre scale was manually cut into the tape using a surgical blade. These features were the following: a single rectangle of 4 mm × 8 mm (Fig. 4a) and 1 mm × 5 mm (Fig. 4b). Feature dimensions were measured using travelling microscope and optical microscope. The tolerance in manual fabrication of these features was found to be ±0.17 mm.

In the next set of experiments, micron scale multiple features were fabricated manually on each anode using the same procedure. The structure consisted of simple features of straight lines and small rectangles shown in Fig. 4c, d respectively. The straight lines were 300 μm thickness and 5.0 mm length. The small rectangles were 500 μm width and 1 mm length. On inspection it was found that the line widths were ± 38.0 μm. Figure 4e and f show optical images of the linear and small rectangle features respectively. A rough and uneven edge of the features was observed which was due to the manual cutting process.

In the last set of experiments, each anode was patterned with features which were within the micrometre range. These were prepared by using standard photolithography with a 0.8–2.4 μm thick photoresist of AZ-5214E (AZ Electronic Materials). The micro pattern structure, shown in Fig. 4g, consisted of vertical and horizontal linear, large square, small square, small circle, as well as some other complex features with an active exposed area of anode was 0.331 cm^2. This feature designs allowed one to examine the possibility of feature replications using Enface in a wide range of feature shapes and sizes.

3.4 Procedure

In order to determine the current for nickel deposition, steady state polarisation data for nickel deposition was determined using Autolabpotentiostat (PGSTAT30) supported by GPES4.9 software. Potentials were scanned cathodically from open circuit potential (OCP) to −1.0 V at scan rate of 2 mV s^{-1}. Polarisation experiments were first carried out using electrodes which had no patterns. Thereafter, another set of experiments were carried out using patterned anodes of 8 mm × 4 mm and 5 mm × 1 mm features. These two set of experiments were carried out to determine if there were any differences in Ni polarisation as features became smaller. The results from these experiments were used to determine an onset nickel deposition potential and optimal current densities for deposition of nickel features.

Pattern transfer experiments were carried out galvanostatically using DC power supplied by using Autolabpotentiostat (PGSTAT30). A current density corresponding to each feature size obtained from polarisation data was used in these experiments at various deposition times between 120 and 600 s (Table 2). The manually fabricated 1 mm × 5 mm features were first used to study the possibility of nickel pattern transfer using Enface technology. A series of deposition experiments using this feature was

Table 2 Summary of pattern features, operating conditions, and results from galvanostatic deposition experiments in 0.19 M nickel sulfamate

Original features	Current density (mA cm^{-2})	Deposition time (s)	Deposited feature width	D/O (%)	Thickness (μm)	Efficiency (%)
Manual millimetre scale width 1.33 ± 0.17 mm	−4.53 ± 0.55	240	1.94 ± 0.23 mm	148 ± 20	0.26	57 ± 4.0
		300	2.34 ± 0.01 mm	179 ± 39	0.31	70 ± 15
		360	2.27 ± 0.02 mm	174 ± 34	0.45	79 ± 3.2
		480	2.59 ± 0.01 mm	198 ± 56	0.54	84 ± 6.3
		600	2.40 ± 0.24 mm	184 ± 43	0.53	62 ± 8.1
Manual micron size						
Rectangle 427.22 μm	−7.59 ± 0.92	125	910 ± 12 μm	213 ± 7.8	0.17	91 ± 14.0
Linear 353.33 μm	−7.59 ± 0.92	125	711 ± 2.0 μm	205 ± 0.5	0.22	91 ± 14.0
Linear 293.30 μm	−7.17 ± 0.92	300	103 ± 41 μm	350 ± 1.0	0.37	90 ± 8.80
Photolithographed micron scale						
Square 803 μm	−1.93 ± 0.46	300	933 ± 62 μm	116 ± 7.7	–	–
Linear 498 μm	−1.93 ± 0.46	300	670 ± 89 μm	135 ± 18	–	–

utilised to understand the process of nickel pattern replication.

The next set of pattern transfer experiments were carried out for the micron scale features which were fabricated manually. These experiments were used to test the performance of Enface for pattern transfer for features within micrometre range. Thereafter, the pattern transfer experiments were carried out for the photo lithographed features. This allowed one to investigate the performance of Enface in a typical pattern transfer condition on a variety of feature shapes and sizes.

Since cell voltage is sensitive to physical changes such as anode passivation, change in nickel concentration, and contamination of the electrode or the solution [16], monitoring the cell potential during pattern transfer process was necessary. The cell potential recorded against time was used to investigate whether the physical changes occurred. Physicochemical properties of the electrolyte were also measured before and after being used for a number of experiments to monitor if significant chemical changes occur in solution.

3.5 Feature size, shape determination, and material characterisation

Dimensions of the nickel deposits (i.e. millimetre scale features) were measured using a travelling microscope (J. Swift & Son series number 29371). Optical microscope and optical profilometer were used to measure deposited features of micron scale. The thickness and the surface profile of the deposits were measured using a Zygo optical surface profiler. For the case of 1 mm × 5 mm features, the entire deposit profile could not be measured since the maximum scanning length of the profiler was less than the width of the feature. In this case only the profile near the deposit edges could be ascertained.

Surface morphology of the deposit was examined by optical microscope and scanning electron microscopy (SEM) to examine if the deposit was dense. Energy dispersive X-ray (EDX) measurements were carried out to investigate if the deposits were metallic. X-ray Photoelectron Spectroscopy (XPS) measurement was carried out to investigate if the diffusion of copper along pores or grain boundaries of the nickel layer occurred.

4 Results and discussion

4.1 Electrolyte formulation

The values of nickel conductivity, as shown in Table 1, show that the experimentally measured conductivity value is lower than the calculated value. This shows that nickel sulfamate is not fully dissociated. However, a pattern replication was expected to be achieved at these conductivity values. The pH of the solutions, as prepared, was in the required range (4–7.5) and no further chemical treatment was necessary.

4.2 Electrochemical characterisation

A set of polarisation experiments were performed on an uncovered nickel anode and patterned anodes at a scan rate of 2 mV s^{-1} and at a gap of 300 μm to determine the potential and an applied current density for nickel deposition. The overpotential was measured against Pt wire reference. The current density was calculated based on the area of the exposed feature on the anode, since the pattern size on the cathode is a priori unknown.

In the case of uncovered electrodes, a typical polarisation curve is characterised by the data presented in Fig. 5 a (curve I). The cathodic region commences at an overpotential of about −0.1 V. The current density slowly increases to reach the first wave, marked (1), at an overpotential of around −0.47 V (see zoom in Fig. 5a′). Thereafter, no increase in current is observed until the potential is significantly high. An increase in current density is observed at overpotentials of around −0.8 V (marked (2)). No Ni was deposited on the electrode before and after (1), but grey Ni was observed after step (2). Hence the onset potential for nickel deposition was estimated to be approximately −0.8 V and above. This suggests that nickel deposition took place through two consecutive one-electron transfer reactions, with (1) corresponding to the first electron transfer (Eq. 3), and (2) corresponding to the second electron transfer (Eq. 5). The plateau region within −0.4 and −0.8 V shows that the first step is mass transfer dependent, in agreement with previous work [43]. The first electron transfer reaction (3) takes place leading to an adsorbed product [43, 44] causing inhibition effect to the second electron transfer reactions [45]. At potential exceeding −1.0 V, hydrogen generation was observed.

As shown in Fig. 5c, in the backward scan when the potential was swept to anodic direction, a single anodic peak is observed at an over potential of −0.37 V. The peak may be attributed to the first oxidation step of nickel dissolution. The intensity of the first anodic peak is much smaller than the nickel deposition. This shows that the deposited nickel oxidation was incomplete due to $Ni(OH)_2$ passivation [43]. A sharp increase of anodic current is observed at potential of around 0.25 V which may represent the subsequent steps of nickel oxidation prior to oxygen evolution.

Polarisation experiments for pattern features of 4 mm × 8 mm and 1 mm × 5 mm were performed to

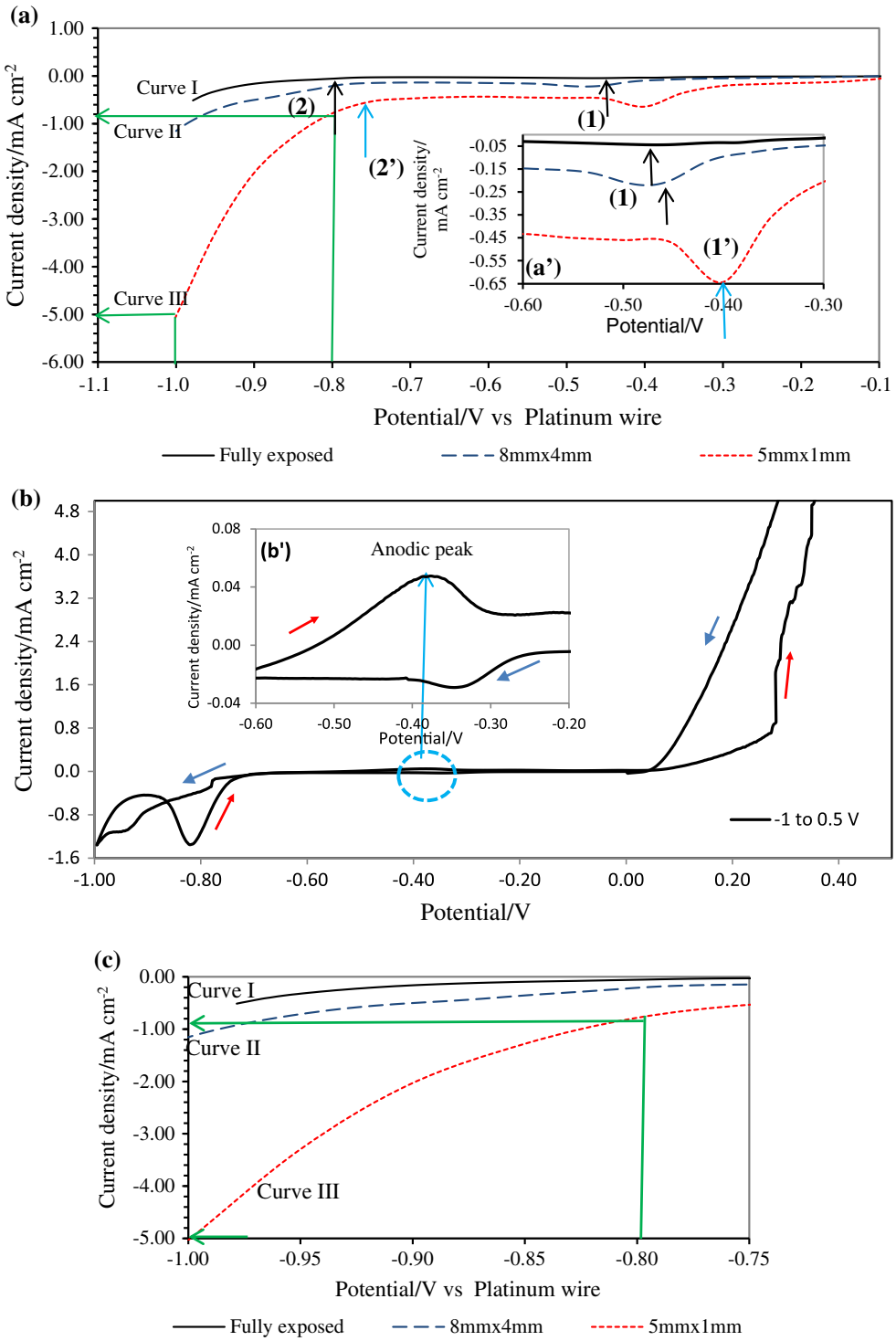

Fig. 5 **a** Cathodicpolarisation curves of nickel in an unstirred 0.19 M nickel sulfamate solution at a scan rate of 2 mVs^{-1} and interelectrode gap of 300 μm on various pattern feature sizes, curve I: uncovered anode, curve II: feature of 4 mm × 8 mm, and curve (III): feature of 1 mm × 5 mm, *arrows* (*1*, *1′*) indicate a peak of first electron transfer and arrows (*2*, *2′*) represent second electron transfer, (*a′*) Zoom in of overpotential range between −0.3 and −0.6 V showing a peak shift of first electron transfer, **b** Cathodic and anodic polarisation curves at 0.5 mVs^{-1} scan rate, and (*b′*) Zoom in of Cathodic and anodic polarisation curves for overpotential range between −0.2 and −0.6 V showing the first anodic peak of nickel oxidation. **c** Zoom in of overpotential region marked 3 between −0.8 and −1.0 V showing the potential and current density range for nickel deposition

investigate whether polarisation behaviour was affected by feature size. The results, shown in Fig. 5a (curve II and III respectively), illustrate similar potential-current density behaviour, although the value of currents for the smaller features is higher. This might be due to the enhancement of diffusional Ni^{2+} mass transfer into a smaller feature as a result of hemispherical diffusion. However, for the 1 mm × 5 mm feature, a potential shift of the first potential wave (Fig. 5a′), from approximately −0.475 V (marked 1) to a more positive value of around −0.40 V (marked 1′), is also observed. The potential of the second step is also shifted from about −0.8 V (marked 2) to around −0.75 V (marked 2′). The cause of this potential shift is unclear. Based on the polarisation measurement

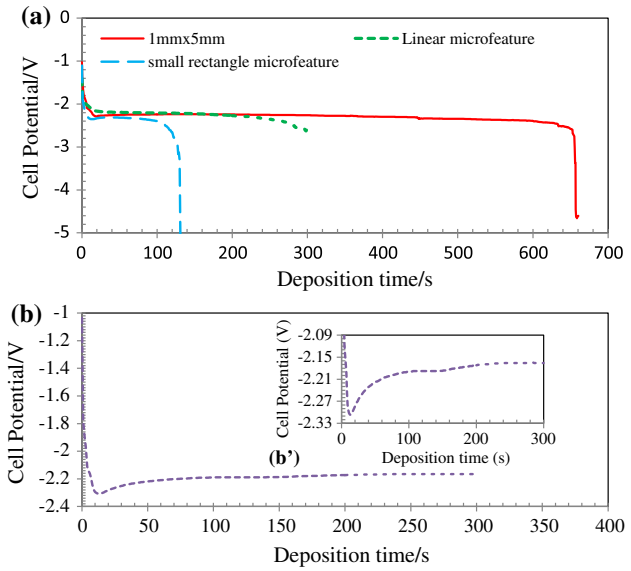

Fig. 6 Cell potential profiles against deposition time of nickel pattern transfer using Enface for **a** various pattern feature sizes and structures which were manually fabricated **b** photolithographed micropattern features structure, (*b*′) *inset* zoom in of potential range where deposition proceeds

(curve III) shown in Fig. 5b, Ni deposition was expected to occur at a potential region of −0.8 to −1.0 V corresponding to a current density range between 0.9 and 5.0 mA cm^{-2}. The patterning experiments for the 1 mm × 5 mm feature were carried out at a current density of 4.53 mA cm^{-2}.

4.3 Electrodeposition

Table 2 lists the applied currents and the cell potential for the pattern transfer experiments. The current densities are different because the feature sizes are different (c.f. Sect. 4.2). No nickel was deposited when the cell potential was below −2.2 V even though an applied current was imposed. This would be expected when only steps 2 and 3 proceed on the cathode surface, but steps 4 and 5 do not. When applied currents higher than those in the Table were used, the cell potential exceeded −2.4 V, and a burnt nickel deposit was obtained. This shows that nickel pattern transfer was achieved at a current density corresponding to a cell potential within the range of −2.2 to −2.4 V.

Based on these findings, cell potential was monitored to investigate whether the physical changes occurred during the deposition process. The results of these potential monitoring is illustrated in Fig. 6a and b which show cell potential against processing times during deposition using manually and photolithographically fabricated anodes.

For deposition experiments using manually fabricated features, immediately after the application of a current, there is an decrease from −1.0 V to approximately −2.2 V. This was used as evidence that nickel deposition was commencing. Thereafter, the cell potential showed a gradual decrease with time, from a value of −2.2 to −2.4 V, when nickel deposition continued. The period of steady decrease in potential was 600 s for the 1 mm × 5 mm (millimetre scale) feature, and about 300 s for the anodes with micron scale features. Following this relatively stable period, there was a rapid decrease in potential again, presumably due to the onset of other reduction reactions, including hydrogen, when the plating experiment was terminated.

The profile for the cell potential for Ni deposition using anodes with micron scale features fabricated by photolithograph were found to be slightly different. There is a slower decrease in the cell potential in the initial period,

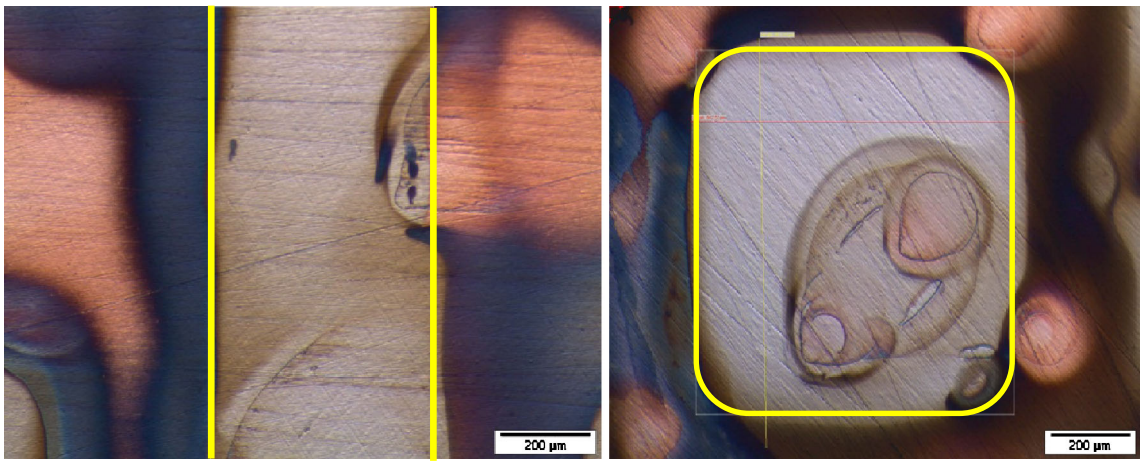

Fig. 7 Deposited cathodes, optical micrograph of deposited features obtained from 0.19 M nickel sulfamate at room temperature (20 ± 2 °C), and stagnant condition for **a** photolithographed linear feature for 300 s, **b** photolithographed large square feature for 300 s

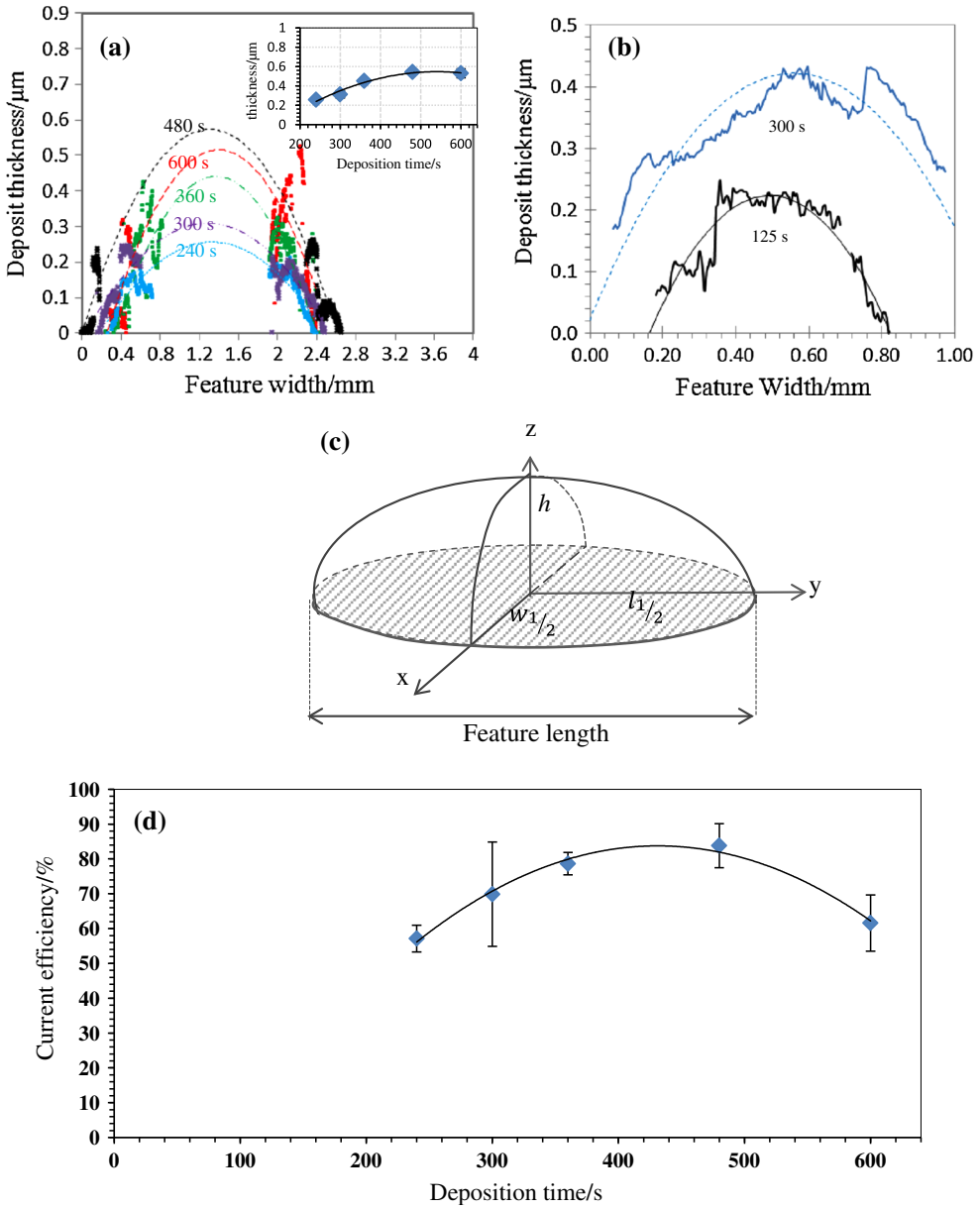

Fig. 8 **a** Profilometer scans showing the thickness, roughness and width of plated nickel pattern obtained from the manual feature of 1 mm × 5 mm at 4.53 ± 0.55 mA cm^{-2} for various plating times, **b** from manually fabricated linear features for 125 and 300 s, **c** a half ellipsoid for estimating the deposited nickel volume, and **d** cathodic current efficiency of nickel pattern deposition from the manual feature of 1 mm × 5 mm for different processing times

reaching maximum, which is followed by slight decrease in cell potential, as is shown in Fig. 6b. A more or less stable cell voltage ranging between −2.2 and −2.4 V is observed thereafter. The sudden decrease to high cathodic voltages was not observed, contrary to the manually fabricated anodes. However, it was also found that the photoresist degraded after a deposition time of 300 s. Due to this problem, for the lithographed anodes, the smaller features were not transferred at all. However, larger linear and square features were deposited, although they remained very thin.

The key issue for all these deposition experiments was that hydrogen evolution or photoresist degradation occurred after a certain period of time. Hydrogen reduction reaction set in as soon as 50 s after commencement of nickel electrodeposition, and clearly after 600 s of deposition, when the cell potential showed a sharp increase. The gas bubbles within the narrow interelectrode gap blocked the electrode surface leading to non-homogeneous nickel deposition [7–9]. In the extreme, it can block the current completely.

The reduction of nickel or hydrogen ion can lead to increase in pH close to the electrode surface. Positive photo-resists are well known to be unstable in alkaline solutions [46, 47]. It is possible that the co-reduction of these species increase the pH during electrodeposition, which leads to photo-resist degradation for the anodes fabricated using photo-lithography, which was observed in these set of experiments.

4.4 Deposit characterisation

4.4.1 Pattern transfer performance

The deposited feature dimensions were measured by using a travelling microscope or an optical microscope. The width was compared to the original feature size to determine the dimensional fidelity of the feature. The increase in feature size is described by a ratio of the width of the deposited feature (D) versus the original one (O). The ratios presented in Table 2 are an average of 5 repetitions. The ratios show that the widths of the deposited nickel features were greater by around 48–98 % for the manually fabricated features of millimetre scale. For the case of micron sized features fabricated manually, the ratio of the deposited vs original width is approximately greater by 105–250 % which indicates that feature broadening is a problem for smaller features. For the lithographed features, since only the large linear and square structures were deposited, these are the only features which were measured. As shown in Fig. 7, the ratio of the deposited features was greater by 16–35 %, substantially less than those fabricated by manual means.

In order to estimate the thickness of the deposits, the deposit profile was assessed using optical profilometry. For the 1 mm × 5 mm feature, the entire surface profile of the features could not be obtained because the maximum width that could be measured was 1 mm. Therefore, the thickness and the surface profile were measured at the two edges of the feature, which are shown in Fig. 8a. As shown in the figure the profile is approximately bell-shaped. The height of the deposited nickel at the centre of the feature measured from the substrate was considered to be the thickness. By assuming a bell-shaped profile across the entire width, a polynomial trend-line was drawn, and the thickness was estimated. The thickness of deposits, as estimated from Fig. 8a, is shown in the inset. The thickness increases at processing times up to 480 s, after which no further increase in thickness is observed. During this period, the average growth rate is 0.072 μm min^{-1}.

For the microscale features fabricated manually, the surface profiles, as measured by an optical profiler are presented in Fig. 8(b). The figure confirms a bell-shaped profile, with both the thickness and the width increasing with time. The thicknesses, as estimated from the bell-shaped curves in Fig. 8b, are also listed in Table 2. The growth in this case is between 0.074 and 0.10 μm min^{-1}, comparable to the millimetre sized features. Since the deposited nickel was very thin for the photolithographed anodes, the thickness could not be measured and hence are not listed.

The volume of the deposit was approximated using a half ellipsoid for the deposits as is shown in Fig. 8c. The volume, V, was calculated using an equation for an ellipsoid (9):

$$V = \frac{1}{2}\left(\frac{4}{3}\pi.l_{1/2}.w_{1/2}.h\right) \tag{9}$$

where h is the deposit thickness on the middle part, $l_{1/2}$ is a half of the feature length, and $w_{1/2}$ is a half of the deposit width. The weight of the nickel deposit was estimated using this volume and a nickel density from literature [48].

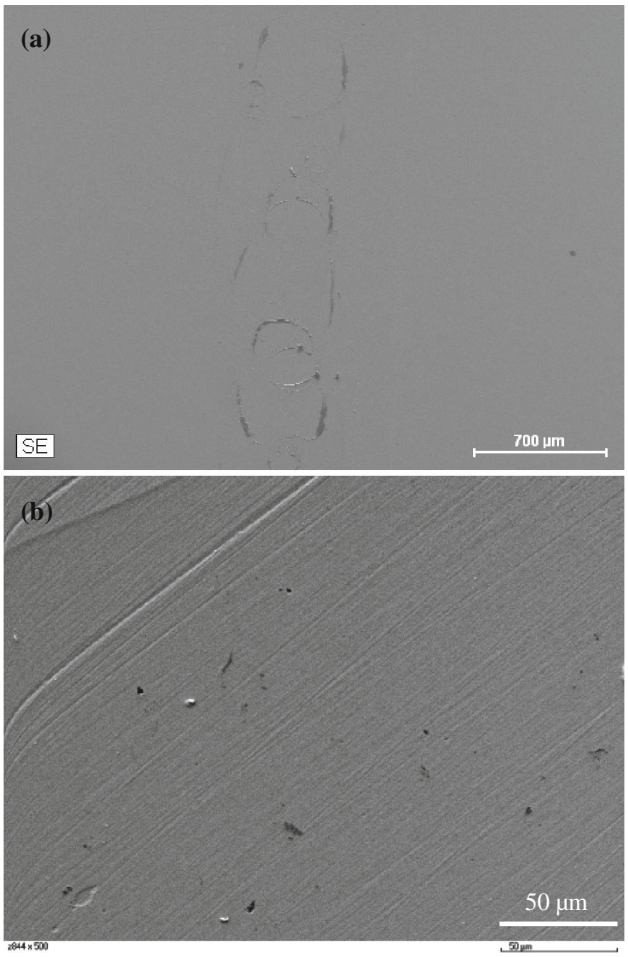

Fig. 9 SEM images of deposited feature obtained from galvanostatic plating on manually fabricated micron scale pattern for linear feature with 260 μm width at −7.17 ± 0.92 mA cm^{-2} for 300 s, **a** at ×50 magnification, and **b** ×2,000 magnification

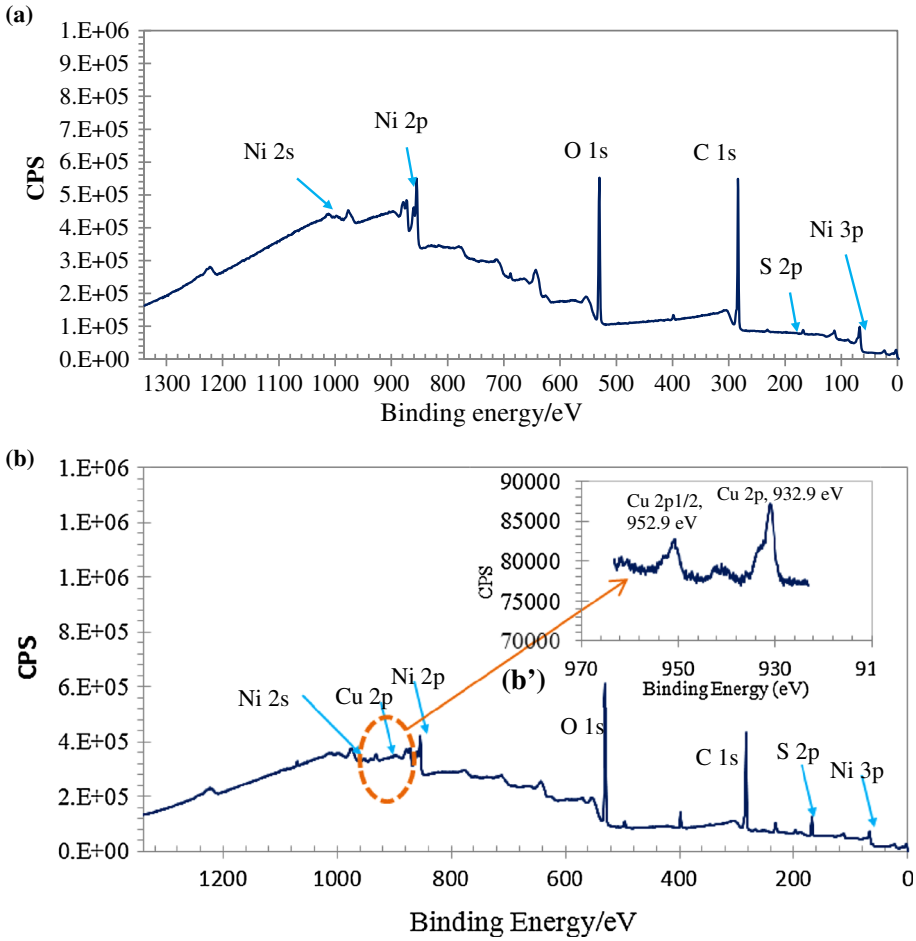

Fig. 10 XPS spectra of nickel feature of 1 mm × 5 mm on copper substrate **a** survey scan for a freshly deposited nickel **b** survey scan of a thermally treated deposited nickel **b′** high resolution scan for copper

A ratio of applied charge and the charge required to obtain the nickel deposit (using Faraday's law) was used to estimate cathodic current efficiency. The last column in Table 2 shows the cathodic current efficiency for nickel deposition. As shown in Fig. 8d, the current efficiency of nickel pattern deposition for 1 mm × 5 mm feature increases as the plating time is increased. Although the efficiency is close to 50 % when plating time is short, it increases to over 80 % if the plating time is lengthened to 480 s. This indicates that the deposition time of around 480 s could be used in subsequent pattern transfer experiments. For the manually-fabricated microscale features, the deposited nickel was achieved with a current efficiency of around 90 % for all cases, much higher than that for the millimetre scale features. This result may be explained by the fact that the current density applied for the micron features was higher than that applied for the millimetre features.

4.4.2 Surface analysis

A further investigation on the morphology of the deposited linear and rectangular features for the manually fabricated features was carried out using scanning electron microscopy (SEM). As shown in Fig. 9a and b, the deposited nickel is observed to be dense and compact.

In order to examine whether the deposited feature was metallic, the samples were investigated by energy dispersive X-ray (EDX). The analysis was carried out on the middle part which exhibit metallic appearance as well as on the edge of the feature which showed a more burnt deposit with black/grey colour. Only peaks for metallic nickel (15.5 %) and copper (84.5 %) were observed on the EDX spectra of the middle part. The EDX spectra of the feature edge revealed that beside nickel (7.03 %) and copper (73.3 %), sulphur (4.2 %) and oxygen (15.5 %) were also present. This is indicative complexing agents (e.g. sulfamate) and nickel oxide are being co-reduced or incorporated.

XPS analysis of the samples was also carried out to determine if they were dense. Figure 10a shows the XPS spectra of the as-deposited nickel. The nickel peaks correspond to metallic nickel, and there are no oxides or sulphur. There is no copper peaks which show that copper does not diffuse from the substrate through the nickel layer. These data corroborate the findings of SEM/EDX analysis that the deposited nickel is not porous.

The second spectrum shows the XPS analysis of a top of the nickel deposit after it has been thermally treated at 100 °C for 100 h (Fig. 10b, b'). The aim of the thermal treatment was to determine if the copper from the underlying substrate can diffuse through the nickel. The XPS spectrum shows the presence of copper at the top of the nickel layer which could diffuse through the deposit at these higher temperatures. When the samples were left at room temperature for a period of 60 days, the spectrum was found to be similar to Fig. 10a, again showing that copper does not diffuse through nickel at lower temperatures. These data also indicate that the deposited nickel is dense and stable at room temperatures.

5 Conclusions

A methodology to carry out nickel deposition using an electrochemical maskless technology, Enface, has been shown. An electrolyte containing 0.19 M nickel sulfamate was found to be suitable, since it fulfilled the requirement of the process. Polarisation experiment for the electrolyte indicated that current density for nickel deposition was different for each pattern feature size. Manually fabricated features of 1 mm × 5 mm have been replicated for deposit thicknesses up to 0.54 μm with a growth of 0.072 μm min^{-1} in the first 480 s. Due to current divergence, the deposited features were found to be 50–100 % wider than the original. For features of around 300 μm, the deposited features are greater by approximately 105–250 %. The growth in this case is between 0.074 and 0.10 μm min^{-1} to achieve a thickness up to 0.37 μm, comparable to the millimetre sized features. The current efficiency was around 90 %. For the lithographed micron scale features, only larger linear and square features of ≥500 μm were deposited, although they remained very thin. The deposited features were greater by 16–35 %, substantially less than those fabricated by manual means. EDX and XPS analysis show that the nickel deposit is metallic. SEM measurement confirms that the deposited nickel was dense and compact. Main issues of the process were the following: (1) hydrogen gas bubbles within the narrow interelectrode gap block the electrode surface causing non-homogeneous nickel deposition and low cathodic current efficiency. In the extreme, the current was completely blocked. (2) The photoresist degraded within the deposition time of 300 s due to hydrogen evolution which led to an increase in pH.

Acknowledgments A grant from Directorate General for Higher Education, Ministry of Education and Culture of Republic of Indonesia through University of Muhammadiyah Surakarta is acknowledged by Tri Widayatno. This work was supported by Royenface Ltd and MESMOPROC (EACI Project#303550). The authors acknowledge National EPSRC XPS User's Service (NEXUS) for XPS measurement and Newcastle University's Advanced Chemical and Materials Analysis (ACMA) unit for SEM and EDX analysis.

References

1. Franssila S (2010) Introduction to microfabrication, 2nd edn. Wiley, West Sussex
2. Madou MJ (2002) Fundamental of microfabrication: the science of miniaturisation. CRC Press, Boca Raton
3. Anwar K, Han T, Kim SM (2010) Sens Actuators B Chem 153(2):301–311
4. Jung E, Ostmann A, Wojakowski D, Landesberger C, Aschenbrenner R, Reichl H (2003) Microsyst Technol 9:449–452
5. Roy S (2010) Innovative electronics Manufacturing Research Centre (IeMRC), 5th annual conference, Loughborough University. Available online at (Accessed 23rd June 2011): http://www.lboro.ac.uk/research/iemrc/documents/EventsDocuments/5th%20Annual%20Conference%202010/Presentations/Roy-Micro%20Pattern%20Transfer%20for%20IeMRC.pdf
6. Roy S (2007) J Phys D Appl Phys 40:413–416
7. SchÖnenberger I, Roy S (2005) Electrochim Acta 51:809–819
8. Wu Q-B, Green TA, Roy S (2011) Electrochem Commun 13(11):1229–1232
9. SchÖenenberger I (2004) Electrochemical microfabrication without photolithography: copper substrates. MPhil thesis, Newcastle University
10. Nouraei S, Roy S (2008) J Electrochem Soc 155(2):D97–D103
11. Roy S (2009) Circuit World 35(3):8–11
12. Shina SG (2008) Green electronics design and manufacturing: implementing lead-free and RoHS-compliant global products. McGraw-Hill Inc., New York, pp 301–304
13. Harper CA (2004) Electronic materials and processes handbook, 3rd edn. McGraw-Hill Inc., New York, pp 612–614
14. Strandjord AJG, Popelar S, Jauernig C (2002) Microelectron Reliab 42:265–283
15. Zhao P et al (2006) IEEE Trans Compon Packaging Technol 29(4):818–826
16. Schlesinger M, Paunovic M (2000) Modern electroplating, 4th edn. In Electrochemical society series. Wiley, New York, pp 139–199
17. Parkinson R NiDI Technical Series No 10 084, Nickel Development Institute
18. Rashidi AM, Amadeh A (2010) J Mater Sci Technol 26(1):82–86
19. Tsuru Y, Nomura M et al (2000) J Appl Electrochem 30(2):231–238
20. Luo JK, Pritschow M, Flewitt AJ, Spearing SM, Fleck NA, Milne WI (2006) J Electrochem Soc 153(10):D155–D161
21. Kelly JJ, Goods SH, Talin AA, Hachman JT (2006) J Electrochem Soc 153(5):C318–C324
22. Gamburg YD, Zangari G (2011) Theory and practice of metal deposition. Springer, New York, pp 291–292
23. Sabine R, Christophe H, Michael M (2005) J Electrochem Soc 152(4):C248–C254
24. Dini JW (1993) Electrodeposition: the materials science of coatings and substrates. Noyes Publication, New Jersey, pp 2–5
25. Hart AC (2011) Trans Ins Met Finish 89(4):181–186
26. Gabe DR, Chen L (2009) Trans Ins Met Finish 87(1):8–10
27. Davis JR (2000) Corrosion: understanding the basics, ASM International, pp 42–44
28. Atkins P, De Paula J (2009) Atkins' physical chemistry, OUP Oxford; 9th edn
29. Pourbaix M (1974) Atlas of electrochemical equilibria in aqueous solution, 2nd English Edition, Houston Tech. National Association of Corrosion Engineering, pp. 331–341

30. Nasirpouri F, Bending SJ, Peter LM, Fangohr H (2011) Thin Solid Films 519:8320–8325
31. Oriňáková R, Turoňová A, Kladeková D, Gálová M, Smith RM (2006) J Appl Electrochem 36:957–972
32. Saraby-Reintjes A, Fleischmann M (1984) Electrochim Acta 29(4):557–566
33. Lantelme F, Seghiouer A et al (1998) J Appl Electrochem 28(9): 907–913
34. Bockris JOM, Drazic D et al (1961) Electrochim Acta 4(2–4):325–361
35. Sasaki KY, Talbot JB (2000) J Electrochem Soc 147(1):189–197
36. Hessami S, Tobias CW (1989) J Electrochem Soc 136(12): 3611–3616
37. Matlosz M (1993) J Electrochem Soc 140(8):2272–2279
38. Fleischmann M, Saraby-Reintjes A (1984) Electrochim Acta 29(1):69–75
39. Epelboin I, Wiart R (1971) J Electrochem Soc 118(10):1577–1582
40. Bozhkov C, Tzvetkova C et al (1990) J Electroanal Chem Interfacial Electrochem 296(2):453–462
41. Nielsen CB, Horsewell A et al (1997) J Appl Electrochem 27(7):839–845
42. Widayatno T, Roy S (2011) Electrodeposition of nickel pattern without photolithography. In: GPE 2011: 3rd international conference on green process engineering, Kuala Lumpur, Malaysia
43. Cui CQ, Lee JY (1995) Electrochim Acta 40(11):1653–1662
44. Albalat R et al (1991) J Appl Electrochem 21(8):709–715
45. Njau KN, Janssen LJJ (1995) J Appl Electrochem 25(10): 982–986
46. Liew MJ, Sobri S, Roy S (2005) Electrochim Acta 51:877–881
47. Liew MJ, Scott K, Roy S (2003) Green Chem 5:376–381
48. Davis JR (2000) Nickel, colbalt and their alloys: 8 (ASM Specialty Handbook), ASM International; Upd Sub edition, pp. 22–112